Mechanism for the Transport of Ammonia within Carbamoyl Phosphate Synthetase Determined by Molecular Dynamics Simulations[†]

Yubo Fan, Liliya Lund, Lijiang Yang, Frank M. Raushel,* and Yi-Qin Gao*

Department of Chemistry, Texas A&M University, College Station, Texas 77843

Received August 6, 2007; Revised Manuscript Received December 14, 2007

ABSTRACT: Carbamoyl phosphate synthetase (CPS) is a member of the amidotransferase family of enzymes that uses the hydrolysis of glutamine as a localized source of ammonia for biosynthetic transformations. Molecular dynamics simulations for the transfer of ammonia and ammonium through a tunnel in the small subunit of CPS resulted in five successful trajectories for ammonia transfer, while ammonium was immobilized in a water pocket inside the small subunit of the heterodimeric protein. The observed molecular tunnel for ammonia transport is consistent with that suggested by earlier X-ray crystallography and site-directed mutation studies. His-353, Ser-47, and Lys-202, around the active site center in the small subunit, function cooperatively to deliver ammonia from the site of formation to the interface with the large subunit, via the exchange of hydrogen bonds with a critical water cluster within the tunnel. The NH_3 forms and breaks hydrogen bonds to Gly-292, Ser-35, Pro-358, Gly-293, and Thr-37 in a stepwise fashion "macroscopically" as it travels through the hydrophilic passage toward the subunit interface. The potential of mean force calculations along the ammonia transfer pathway indicates a low free-energy path for the translocation of ammonia with two barriers of 3.9 and 5.5 kcal/mol, respectively. These low free-energy barriers are consistent with the delivery of ammonia from the site of formation into a water reservoir toward the exit of the tunnel and migration through the hydrophilic leaving passage, respectively. The high overall free-energy barrier of 22.4 kcal/mol for the transport of ammonium additionally substantiates that the tunnel in the small subunit of CPS is not an ammonium but an ammonia channel.

Carbamoyl phosphate synthetase (CPS)[1] plays a critical role in the biosynthesis of pyrimidine nucleotides and the detoxification of ammonia. The enzyme from *Escherichia coli* catalyzes the synthesis of carbamoyl phosphate from bicarbonate, glutamine, and two molecules of ATP via a chemical mechanism that involves four separate reactions and three unstable intermediates (*1*). In the first step, ATP is used to phosphorylate bicarbonate to generate a carboxy phosphate intermediate. Glutamine is hydrolyzed to glutamate and ammonia, and then the ammonia subsequently reacts with carboxy phosphate to produce the third intermediate, carbamate. In the final step, the second ATP phosphorylates carbamate to form the ultimate product, carbamoyl phosphate. The reaction mechanism is summarized in Scheme Scheme 1.

Scheme 1

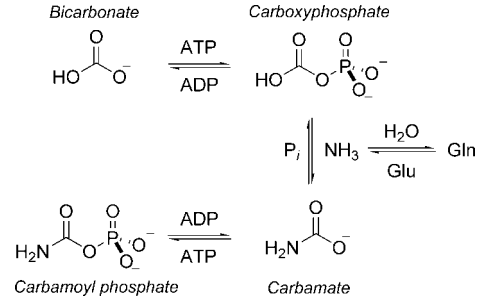

The *E. coli* enzyme is comprised of two subunits of molecular weight ~40 and ~118 (*2*). The smaller of the two subunits contains the binding site for the hydrolysis of glutamine, whereas the large subunit catalyzes the formation of carbamoyl phosphate (*3*). The three-dimensional X-ray structure of CPS has revealed the location of three spatially distinct active sites (*4*). The small subunit contains the active site for the hydrolysis of glutamine, and the N-terminal domain of the large subunit possesses the active site for the formation of carboxy phosphate and carbamate. The third active site is located within the C-terminal domain of the large subunit, and it catalyzes the phosphorylation of carbamate. The three active sites are connected by two intramolecular tunnels that extend nearly 100 Å from one end of the protein to the other (*4*). The "ammonia tunnel" starts at the active site in the small subunit and leads to the active site in the N-terminal domain of the large subunit. This tunnel functions to facilitate the migration of ammonia from the site of production to the site of use. The "carbamate tunnel" connects the two active sites within the large subunit

[†] This work was supported in part by the Robert A. Welch Foundation (A-840 to F.M.R. and A-1628 to Y.-Q.G.) and the National Institutes of Health (NIH, R56 DK030343 to F.M.R.). The supercomputer facilities at Texas A&M University were supported by the National Science Foundation (NSF, NSF-DMS 0216275). Y.-Q.G. is a 2006 Searle Scholar.

* To whom correspondence should be addressed. Telephone: (979) 845-3373. Fax: (979) 845-9452. E-mail: raushel@tamu.edu (F.M.R.); Telephone: (979) 458-0592. Fax: (979) 845-4719. E-mail: yiqin@mail.chem.tamu.edu (Y.-Q.G.).

[1] Abbreviations: CPS, carbamoyl phosphate synthetase; MD, molecular dynamics; PMF, potentials of mean force; WHAM, weighted histogram analysis method; PDB, Protein Data Bank; IGPS, imidazole glycerol phosphate synthase.

10.1021/bi701572h CCC: $40.75
Published on Web 01/26/2008

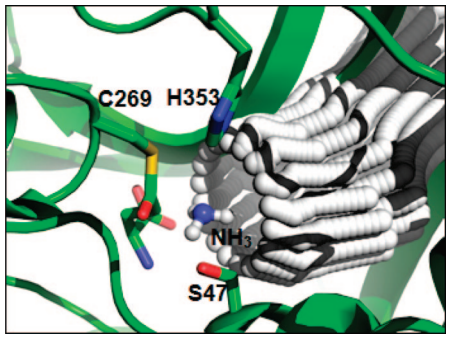

FIGURE 1: Active site for the hydrolysis of glutamine in the small subunit of CPS and the proposed tunnel for the translocation of ammonia. Cys-269 was computationally modified as a γ-glutamyl thioester intermediate. Nitrogen, oxygen, hydrogen, and carbon atoms are shown in blue, red, white, and cyan, respectively. The white spheres illustrate the approximate boundaries for the ammonia tunnel (*4*). The image was constructed from PDB file 1C3O.

to one another and guides the unstable carbamate intermediate to the site of phosphorylation.

The existence of intramolecular tunnels has been found in all members of the amidotransferase family of enzymes for which structural information is available (*5*). From these X-ray structures, it is apparent that the catalytic machinery for the hydrolysis of glutamine to ammonia has been conserved. However, the structural architecture for the tunnel that facilitates the movement of ammonia from one active site to the next has apparently evolved independently in each case. Isotopic labeling studies have demonstrated that the ammonia produced from the hydrolysis of glutamine in CPS does not exchange with unlabeled ammonia in the bulk solution (*6*). Therefore, the wild-type enzyme is not leaky, and the reactions are highly coupled with one another. The functional significance of the ammonia tunnel in CPS has been demonstrated by the construction of mutant enzymes that result in the leakage of ammonia directly into the bulk solution through a perforation in the tunnel wall (*7, 8*). In the G359F mutant of the small subunit of CPS, the molecular hole has been verified by X-ray crystallography.

In the active site of the small subunit, there is a constellation of three amino acid residues that are critical for the hydrolysis of glutamine (*9*). A thioester intermediate is formed through the nucleophilic attack of Cys-269 on the carboxamide moiety of glutamine. This cysteine residue is activated via a proton transfer from the thiol group to the imidazole side chain of His-353. The tetrahedral intermediate is stabilized through a hydrogen-bonding interaction with the side-chain hydroxyl of Ser-47. The collapse of the tetrahedral intermediate is facilitated by a proton transfer from His-353 to the $-NH_2$ substituent to generate ammonia in the active site. Ammonia is apparently injected into the tunnel, and the thioester intermediate is subsequently hydrolyzed. Experimental support for the putative tetrahedral intermediate has come from the X-ray structure of the enzyme in the presence of a glutamate γ-semialdehyde inhibitor (*10*). The thioester intermediate has been trapped in the H353N mutant in the presence of added glutamine (*10*). The structure of the thioester intermediate and the other active site residues are highlighted in Figure 1.

The ubiquitous existence of intramolecular protein tunnels connecting spatially distinct active sites in enzymes has been revealed via high-resolution X-ray crystallography and further confirmed by site-directed mutations. Some of the key residues for the chemical transformations in these enzymes have been identified, but the dynamics and mechanism for the transfer of reaction intermediates through these molecular tunnels have not been observed directly. Therefore, in this investigation, molecular dynamics (MD) simulations were conducted to articulate the interactions between the substrate and protein environment within the molecular tunnel at the atomic level and to obtain the free-energy profile for the transport of ammonia. MD simulations have previously been applied to the problem of ammonia transport in proteins. For example, the transfer of NH_3 in imidazole glycerol phosphate synthase (IGPS) was studied using steered MD (*11, 12*). The free-energy profile for NH_3 transfer in AmtB was calculated with the umbrella sampling technique (*13, 14*), and this system was also investigated using conventional MD simulations at a temperature of 323 K (*15*). In particular, the free-energy profiles for the transfer of NH_3 and NH_4^+ through the AmtB membrane protein indicated that NH_3 travels through this tunnel quite easily with an overall barrier of about 6 kcal/mol, while NH_4^+ is prevented from passing by a barrier of at least 25 kcal/mol (*13*). The dehydration of NH_4^+ is much less favored than that for NH_3 when they are transported through the relatively narrow tunnel (*13*). However, to the best of our knowledge, the spontaneous transport of NH_3 has not been observed previously by normal MD simulations at room temperature. In all of the earlier studies, artificial forces were introduced to accelerate the transport of NH_3 and NH_4^+. These forces include steered MD, umbrella sampling techniques, and simulating the transport at higher temperatures.

Here, we report the mechanism for the transport of NH_3 through the small subunit of CPS as determined by MD simulations without introducing any artificial forces. A mechanism is given for the translocation of NH_3 through the small subunit portion of the molecular tunnel, which connects the active site for the hydrolysis of glutamine to the active site for the synthesis of two reactive intermediates, carboxyphosphate and carbamate. In addition, free-energy profiles for ammonia and ammonium transport were obtained using the umbrella sampling technique. These studies demonstrated that NH_3 but not NH_4^+ is the actual species that migrates through the tunnel. These calculations also revealed the functional significance of water molecules in the ammonia tunnel and a conformational rotation of the imidazole side chain of His-353 that initiates the injection of ammonia into the molecular tunnel.

MATERIALS AND METHODS

Construction of Models for the Thioester Intermediate. Chain B in the X-ray crystal structures of CPS (PDB codes 1C3O and 1CS0) was taken as the starting point for the simulations of NH_3 transfer in the small subunit of CPS (*10*). The residues Met-1, Ala-381, and Lys-382 are missing in these X-ray structures, and they were not included in the simulations. A molecule of glutamine is bound in the active site of the small subunit of CPS for the mutant C269S (1C3O). The replacement of Cys-269 with a serine residue results in a protein that is able to bind glutamine but unable to hydrolyze the amide bond. In this mutant, His-353 is apparently unable to activate the hydroxyl group of the serine,

so that the glutamine is bound within the active site instead of being hydrolyzed. In the PDB file 1CS0, the wild-type CPS is bound with a glutamate γ-semialdehyde inhibitor in the active site of the small subunit. In this structure, the thiol group of Cys-269 has formed a covalent bond with the side-chain aldehyde group to generate a tetrahedral addition complex that mimics the proposed tetrahedral intermediate that occurs during amide bond hydrolysis. In the simulations reported here, Ser-269 with the bound glutamine in the C269S mutant (1C3O) and the covalently bonded inhibitor with Cys-269 in the wild-type CPS (1CS0) were replaced with a γ-glutamyl cysteine residue (Cyg). The geometry of the Cyg group was optimized to a local minimum, and the conformation was kept consistent with the substituted Cys-269 of the wild-type CPS (1CS0).

The charge distributions on all atoms in Cyg, NH_3, and NH_4^+ were obtained using the RESP-fit method (*16, 17*) based on B3LYP/cc-pVTZ calculations (*18–21*) with the solvent effect ($\epsilon = 4$) included using the polarizable continuum model (*22–24*). The geometries for NH_3 and NH_4^+ were fully optimized in the gas phase at the same level as that for the charge distribution calculations and positioned between the sulfur in Cyg-269 and His-353. The charges on the nitrogen atom in NH_3 and NH_4^+ are -0.9882 and -0.8022, respectively. All crystalline waters in the small subunit or on the protein exterior were kept, and all ions (K^+ and Cl^-) around the subunit were removed. The net negative charge was neutralized by added Na^+ ions. Explicit TIP3P waters (*25*) were added as a truncated octahedral water box with an 8 Å buffer. All operations were processed using AMBER Leap module (*26, 27*), which led to four basic systems: 1C3O plus NH_3, 1CS0 plus NH_3, 1C3O plus NH_4^+, and 1CS0 plus NH_4^+ with 38 106, 39 066, 37 308, and 38 310 atoms, respectively. In addition, the side chain of His-353 has two potential orientations, where either N_δ or N_ϵ pointing toward Cyg-269. Because either N_δ or N_ϵ can be protonated, there are thus four candidates for the conformation and protonation state of His-353 in the MD simulations. The four structures, in which N_ϵ is protonated with N_ϵ pointing toward Cyg-269, N_δ is protonated with N_δ pointing toward Cyg-269, N_ϵ is protonated with N_δ pointing toward Cyg-269, and N_δ is protonated with N_ϵ pointing toward Cyg-269, are defined as E1, D1, E2, and D2, respectively. Besides E1 (two systems for the NH_3 transfer mentioned above), structures with a NH_3 added to the active site were also created for D1 and D2 with 39 066 and 39 066 atoms, respectively. The systems were further extended using the periodic boundary condition. The Amber force field 99 (*28*), with the parameters for the peptide backbone reoptimized (*29*), was used for all standard amino acid residues, NH_3, and NH_4^+, while the general AMBER force field (*30*) was used for the sulfur-related bonds, bond angles, and torsional angles in the γ-glutamyl thioester (Cyg). MD simulations were conducted in the isothermal–isobaric ensemble at 300 K and 1 atm. The SHAKE algorithm was used to constrain all bonds involving hydrogens (*31*). A 10.0 Å cutoff was applied for nonbonding interactions. The particle mesh Ewald method was employed to treat the long-range electrostatic interactions (*32, 33*).

MD trajectories were obtained on these structures using the AMBER suite of programs (*26, 27*). Before the MD simulations, in which the trajectories were collected every 0.5 ps, two steps of minimization were conducted. During the minimization, the systems were first optimized for 1000 cycles, while the backbone of the protein was frozen with a force constant of 500.0 kcal/mol. The systems were then further optimized for 2500 cycles without constraints, followed by a 20 ps MD simulation for heating the system from 0 to 300 K, with a force constant of 10.0 kcal/mol upon all 379 amino acid residues. Two successful trajectories of 14 (1C3O) and 9.5 (1CS0) ns, in which NH_3 transfers out of the small subunit in 12.8 and 7.3 ns, respectively, were obtained for the E1 structure, while NH_4^+ was trapped in the protein in two 40 ns trajectories (from 1C3O and 1CS0).

Free-Energy Calculations. The reaction coordinate for the free-energy simulations was defined from the carbonyl carbon of the thioester intermediate in Cyg-269 to the hydroxyl oxygen of Thr-37, which is positioned at the interface between the small and large subunits of CPS. The free-energy profiles or potentials of mean force (PMF) were computed along the translocation trajectories using the umbrella sampling technique with a biasing harmonic potential involving a force constant of 20 kcal/mol (*34–38*). The PMF for NH_3 transfer was calculated with 71 windows chosen from the 14 ns trajectory, while the PMF for NH_4^+ was performed with 38 windows referring to the former trajectory. For each window, a 10 ps equilibration simulation was performed first and a subsequent 400 ps simulation generated dynamics data for the weighted histogram analysis method (WHAM) analyses (*35–37*).

RESULTS AND DISCUSSION

Translocation of NH_3 in the Small Subunit. In the simulation of the wild-type CPS, a net movement of about 13 Å was observed for the transfer of NH_3 in the two successful trajectories for the E1 structure, lasting 14 and 9.5 ns, respectively. This is apparently the first time that a tunnel for the transfer of NH_3 in an enzyme has been confirmed by MD simulations at room temperature without applying any artificial forces. The protein tunnel originally observed in the X-ray crystal structure of CPS is apparently the lowest free-energy path for the translocation of NH_3. In the two trajectories, the NH_3 translocates out of the protein and solvates with the bulk water at 12.8 and 8.9 ns, respectively. The movement of NH_3 in these simulations occurs in approximately three stages. In the first stage, the NH_3 is directed away from the thioester intermediate and into the tunnel by the combined action of His-353 and Lys-202. The NH_3 then travels toward the large subunit through positional exchange with multiple water molecules located in the tunnel, and finally, the NH_3 exits the small subunit through a hydrophilic passage at the subunit−subunit interface.

Several typical structures along the 14 ns trajectory for the E1 structure are shown in parts A−F of Figure 2. At the beginning of the trajectory, the NH_3 oscillates between the thioester intermediate and His-353 by exchanging hydrogen bonds with His-353, Ser-47, and several water molecules. The NH_3 is constrained within the active site by two hydrogen bonds to His-353 and Ser-47 as shown in Figure 2A. The hydrogen bond to His-353 appears to be important because the NH_3 would not be delivered into the tunnel if this hydrogen bond is not formed. The NH_3 is initially placed

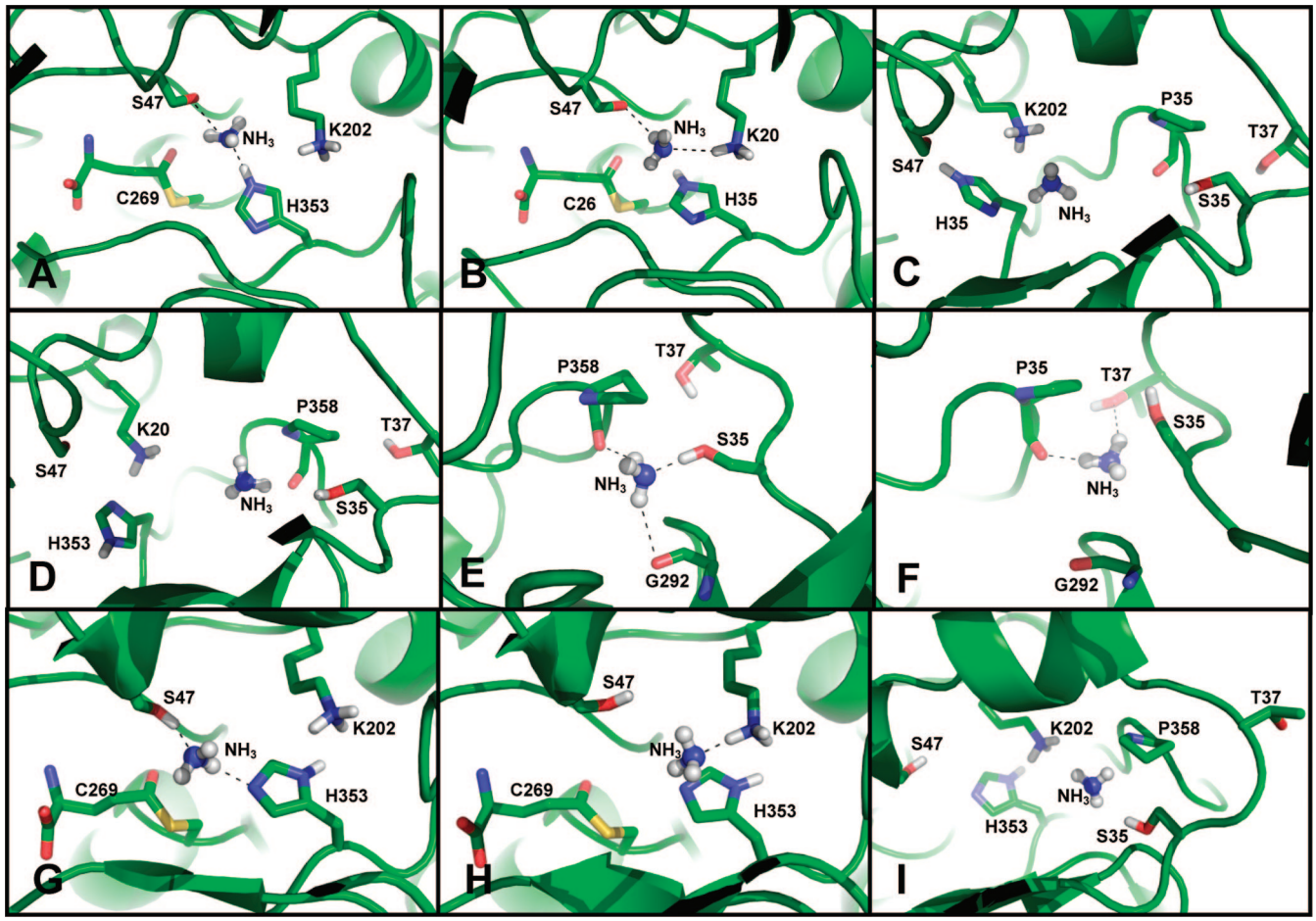

FIGURE 2: Snapshots of NH_3 and nearby residues in the 14 ns MD trajectory for the E1 structure (A−F) and the first-step section of the trajectory for the D2 structure (G−I). The dashed lines represent hydrogen bonds. R = 4.58 Å (A), 4.55 Å (B), 7.88 Å (C), 10.64 Å (D), 12.75 Å (E), and 15.71 Å (F). R represents the distance between the nitrogen atom of NH_3 and the carbonyl carbon of the thioester intermediate in Cyg-269. R = 3.27 Å at 75.5 ps (G), 6.12 Å at 0.29 ns (H), and 11.46 Å at 0.57 ns (I) for the D2 trajectory.

between Cyg-269 and His-353, and the initial distance between the nitrogen atom of NH_3 and either of the nitrogen atoms in the imidazole group of His-353 is longer than 3.5 Å. Thus, in the initial setup, the NH_3 could migrate to other residues instead of His-353 or be lost to the solvent at the beginning of the trajectory if the hydrogen bond between the NH_3 and His-353 does not form (data not shown). A hydrogen bond between ammonia and the side chain of His-353 was observed in all of the successful trajectories whatever the initial structure, such as D1 and D2 described in the computational details. However, this hydrogen bond must occur when the NH_3 is initially formed from the tetrahedral intermediate because one of the three protons in the NH_3 is delivered directly from the side-chain imidazole of His-353. Consequently, the amino group of the tetrahedral intermediate and the imidazole group of His-353 switch between a N−H covalent bond and a hydrogen bond during the proton transfer. Furthermore, this hydrogen bond is unable to break easily because Ser-47 forms an additional hydrogen bond with the NH_3 after the collapse of the tetrahedral intermediate during the hydrolysis of glutamine. To be precise, even if His-353 changes its conformation or protonation state of the side chain, the ammonia is still detained around it by Ser-47. The hydrogen bond easily forms again between the ammonia and His-353. The situation that the hydrogen bond to His-353 breaks while that to Ser-47 remains was observed in all trajectories of D1, D2, E1, and E2 configurations, although the probability for the ammonia forming two hydrogen bonds to His-353 and Ser-47 is much higher in the sections before the ammonia moves into the water pocket in the middle. These hydrogen bonds constrain the space for the NH_3 and thus enforce the binding of the NH_3 to His-353 and prevent the NH_3 from escaping to anywhere other than the molecular tunnel.

The movement of the ammonia into the tunnel is initiated by the hydrogen bond with the imidazole group of His-353 with the attachment of NH_3. A new hydrogen bond forms between NH_3 and Lys-202 with the breaking of the original hydrogen bond between the NH_3 and His-353, while the interaction with Ser-47 remains intact (Figure 2B). The cluster of water molecules in the tunnel begins to interact with the NH_3, while the hydrogen bond to Ser-47 weakens and finally breaks (Figure 2C). Additional waters from the cluster begin to attract the NH_3, resulting in the ultimate liberation of the NH_3 from the hydrogen bond with Lys-202 (Figure 2D). The flexibility of the Lys-202 side chain allows for the delivery of NH_3 deep into the water cluster and completes the hydration of NH_3. The NH_3 moves gradually toward the hydrophilic exit within the interior pocket containing a cluster of water molecules, by exchanging hydrogen bonds with successive water molecules and the surrounding residues. Ultimately, the NH_3 reaches the distal side of the pocket and binds to the hydroxyl side chain of Ser-35 and the backbone carbonyl groups of Gly-292 and

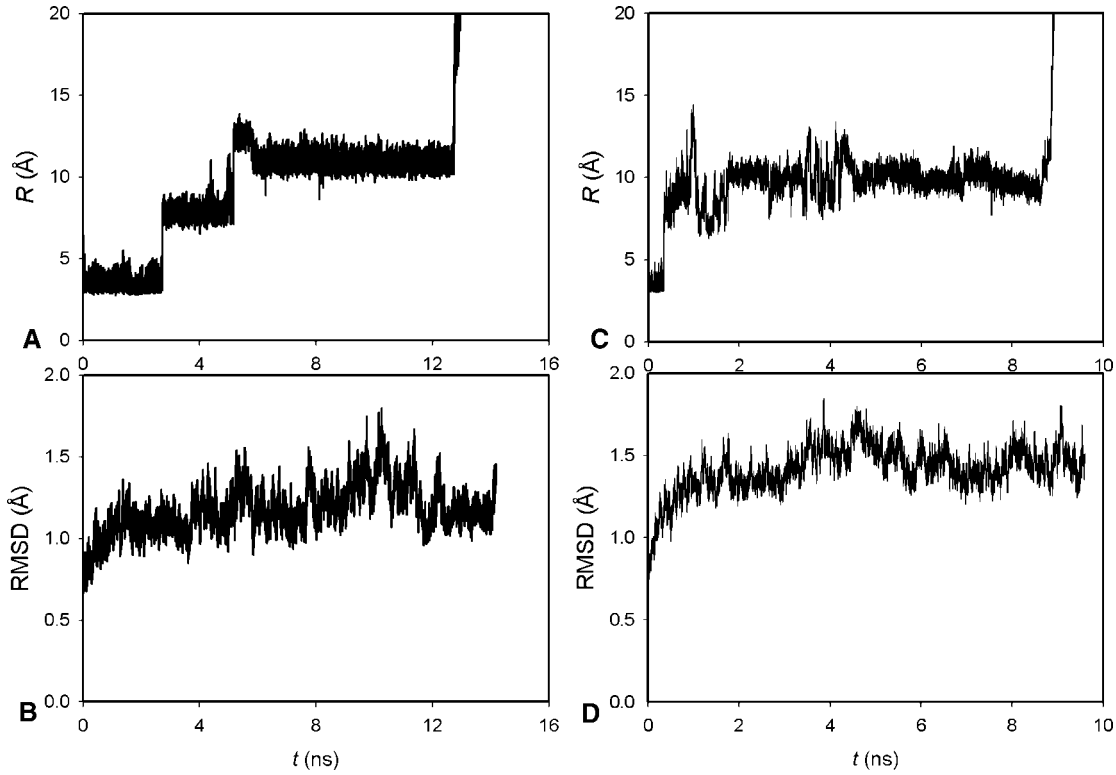

FIGURE 3: Distance (*R*) between the nitrogen of NH_3 and the carbonyl carbon of the thioester intermediate in Cyg-269 (A) and rmsd of the CPS small subunit backbone (B) in the 14 ns trajectory and the distance (*R*) (C) and rmsd (D) in the 9.5 ns trajectory.

Pro-358. Three new hydrogen bonds are formed in this process as shown in Figure 2E. The side chain of Ser-35 subsequently rotates about the C−C bond by ∼150° and tilts away from the exit to deliver the NH_3 further into the tunnel. The hydrogen bond between NH_3 and Ser-35 breaks as a new hydrogen bond begins to form with the hydroxyl group of Thr-37 (Figure 2F). Then, the NH_3 frequently forms and breaks hydrogen bonds with the backbone substituents of Pro-358, Gly-293, and Thr-37 and ultimately approaches the end of the tunnel in the small subunit. Actually, it is observed that the ammonia hydrogen bonds to P358, G293, and T37 simultaneously in the successful trajectories, and this hydrogen-bond network is very likely the initial force for the traveling of NH_3 through the hydrophilic exit. At the interface between the large and small subunits of CPS, the NH_3 has traveled about 13 Å through the tunnel during this simulation.

The 14 ns trajectory described above exhibits a three-stage transport of NH_3 that is quantified by the distance (*R*) between the nitrogen atom of NH_3 and the carbonyl carbon of the thioester intermediate in Cyg-269 as a function of the simulation time (Figure 3). During the simulation, the protein conformation of the small subunit of CPS is quite stable and the root-mean-square deviation (rmsd) of its backbone atoms is 1.18 Å on average with a 1.80 Å maximum as shown in Figure 3B. The first stage, lasting about 2.7 ns, corresponds to the oscillation of NH_3 within the region surrounded by Cyg-269, His-353, and Ser-47. After 2.72 ns, the NH_3 shifts with the rotational assistance of the His-353 side chain and the distance *R* increases by about 4 Å (step one). After a "quiet" period of about 2.5 ns, *R* fluctuates at around 8 Å. During this period of time, the NH_3 is trapped in the region encircled by His-353, Ser-47, and Lys-202. A subsequent shift of 4 Å in *R* (step two) is then observed at 5.18 ns. This change in *R* is the direct result of NH_3 dissolving within the water cluster and migration to the inner portion of the hydrophilic passage. In the next stage, lasting more than 10 ns, the water cluster stabilizes and pulls the NH_3 back to the middle of the water pocket. At 12.74 ns, the NH_3 finally accesses the passage and traverses through it in 10 ps by covering a distance of about 6 Å. Finally, the NH_3 leaves the small subunit and solvates into the bulk water solution.

In general, the movement of NH_3 in the 9.5 ns trajectory is similar to that in the 14 ns trajectory. However, the distance *R* changes in a more complicated fashion in this trajectory (Figure 3C). In the beginning of this trajectory, the NH_3 passes His-353 at 0.34 ns and then oscillates in the region between His-353 and Lys-202. NH_3 gradually travels to the water pocket with a hydrogen bond to Lys-202 in the time period from 0.35 to 0.85 ns. Analogous to the 14 ns trajectory, the NH_3 then travels quickly to the inner portion of the hydrophilic passage during the next 0.1 ns. However, the water cluster again withdraws the NH_3 back to the pocket because of the considerable stabilization by solvation. The NH_3 moves back toward His-353 and Lys-202 and oscillates between these two residues from 1.1 to 1.7 ns. The NH_3 then re-enters the water pocket but frequently moves back and forth and oscillates between Ser-35 and His-353, especially in the time period of 3.6−4.4 ns. This motion lasts for about 8.5 ns in total until the NH_3 finally infiltrates the hydrophilic passage at 8.88 ns. The protein conformation is stable during this simulation. The rmsd of the backbone is 1.42 Å on average with a 1.85 Å maximum as shown in Figure 3D.

Effects of Water Molecules. From the structures obtained in the two successful trajectories, it is found that the cluster of water molecules is crucial for the effective transfer of NH_3 within the tunnel. The sites vacated by NH_3 with broken hydrogen bonds are refilled by water molecules in the tunnel,

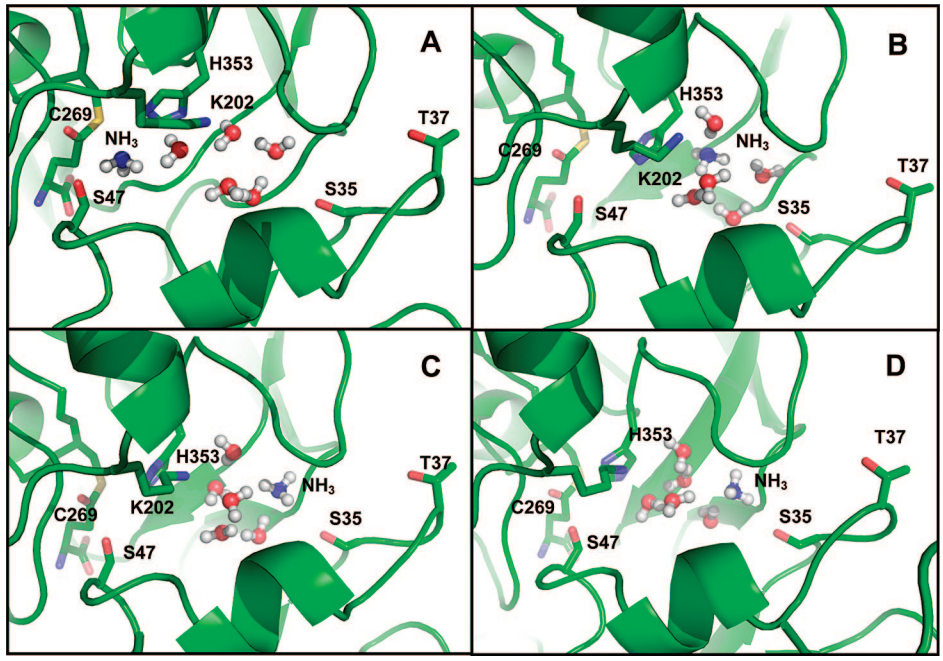

FIGURE 4: NH_3 surrounded by a water cluster at 2 ns (R = 3.68 Å) (A), 4 ns (R = 8.64 Å) (B), 8 ns (R = 11.39 Å) (C), and 12 ns (R = 11.59 Å) (D) in the 14 ns trajectory.

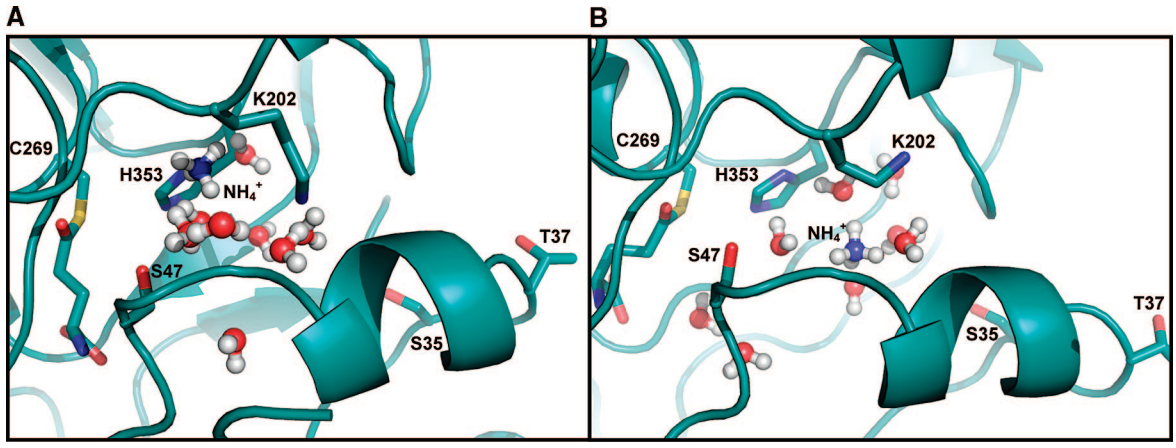

FIGURE 5: NH_4^+ surrounded by a water cluster at 2 ns (R = 6.96 Å) (A) and 15 ns (R = 8.50 Å) (B) in the 40 ns trajectory.

so that the original hydrogen bonds are unable to form again. In this sense, the water molecules in this cluster catalyze the breaking of the hydrogen bonds between NH_3 and the side chains of His-353, Lys-202, and Ser-47, and thus, the NH_3 is able to move progressively forward instead of oscillating back and forth and remaining perpetually stuck within the small subunit. The NH_3 travels from the active site to the final exit passage in the small subunit of CPS, and the typical water-surrounding structures are shown in Figure 4. The NH_3 is bound first by His-353 and Ser-47 with two hydrogen bonds, while it starts to interact with the cluster of five waters (Figure 4A). The NH_3 is then solvated by the water cluster (Figure 4B) and subsequently migrates to the other side of the water pocket (Figure 4C). The ammonia finally passes through the hydrophilic exit with a hydrogen bond to Ser-35 (Figure 4D). The immobilization of the NH_3 between His-353 and Ser-47 in another trajectory lasting 10.15 ns (not shown and similar to Figure 4A) indicates that the hydrogen-bond network is considerably stable, so that the NH_3 is unable to travel into the water pocket without the exchange of hydrogen bonds within the water cluster.

Translocation of NH_4^+ in the Small Subunit. The MD simulations demonstrate that NH_4^+ is incapable of traveling through the tunnel and out of the small subunit of CPS. In two 40 ns trajectories, the NH_4^+ transfers from the active center to the water cluster relatively quickly. During the two initial steps of minimization, the NH_4^+ has rapidly moved to a position between His-353 and Lys-202, although NH_4^+ does not interact with Lys-202 by forming a hydrogen bond (Figure 5A). Very likely, this movement occurs at the starting point because of the relatively weak attraction between NH_4^+ and Cyg-269 and the strong solvation from the waters in the water pocket (Figure 5B). In both trajectories, the NH_4^+ does not interact with Ser-35 effectively and fails to enter the hydrophilic passage mentioned above. Although NH_4^+ could form hydrogen bonds with the residues in the hydrophilic passage, this ion is likely prevented from desolvating from the water pocket because NH_4^+ gains a much higher solvation energy in water relative to NH_3. In the narrow hydrophilic passage, the total number of hydrogen bonds will be limited for both NH_4^+ and NH_3. As a result, NH_4^+ is much more destabilized in the hydrophilic passage than NH_3.

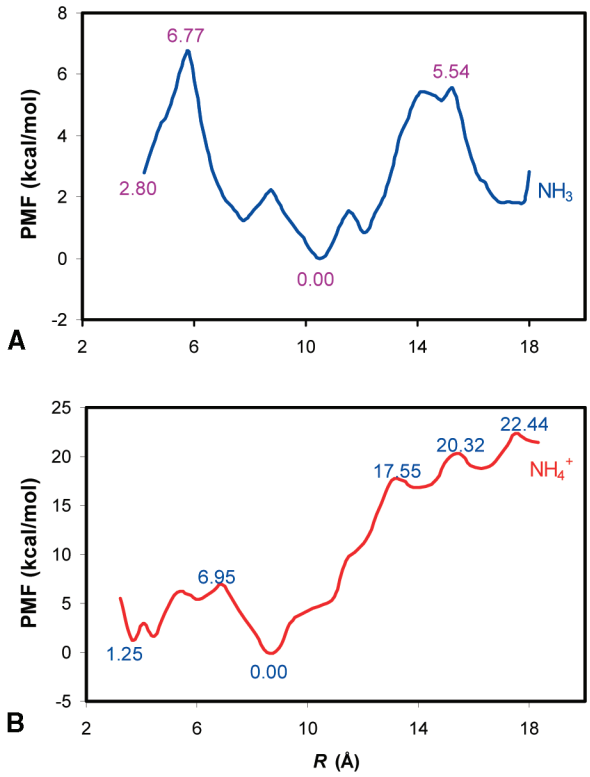

FIGURE 6: PMF profiles for the translocation of NH_3 (A) and NH_4^+ (B) along the tunnel in the CPS small subunit. The lowest point in each profile is defined as zero energy. The reaction coordinate *R* is the distance between the nitrogen in NH_3/NH_4^+ and the carbonyl carbon bonding to the sulfur in Cyg-269.

Free-Energy Profiles. To understand the mechanism of NH_3/NH_4^+ transfer and the interactions between NH_3/NH_4^+ and the surroundings, the PMF along the reaction coordinate in the tunnel was calculated using the umbrella sampling technique. The PMF profiles are shown for NH_3 transfer in Figure 6A and indicate an approximate two-step process with barriers of 3.9 and 5.5 kcal/mol, respectively, which appear at the distance *R*, between NH_3 and Cyg-269, of 6.0 and 14.3 Å, respectively. The first barrier is consistent with the transfer of NH_3 from Cyg-269 to Lys-202 by the rotation of the His-353 side chain. The second barrier is related to the delivery of NH_3 from the water pocket to the exiting passage by the rotation of Ser-35. The barrier at *R* of 5.8 Å refers to the breaking of the hydrogen bond between NH_3 and the imidazole side chain of His-353, while the hydrogen bond between NH_3 and Ser-47 remains intact. The small barriers at 8.7 and 11.5 Å are likely related to the breakage of the hydrogen bond between NH_3 and Lys-202 when NH_3 enters the water pocket and the exchange of hydrogen bonds between NH_3 and surrounding waters or amino acid residues, although no specific interactions were observed in the simulations. The plateau at ~5.5 kcal/mol, at a distance *R* of 14−16 Å, corresponds to the desolvation of NH_3 from the water cluster and movement toward the hydrophilic exit. After Ser-35 is passed, NH_3 moves quickly out of the small subunit of CPS as a result of the steep downhill trajectory in the free-energy profile after 15.3 Å (see Figure 6A). It is important to note that there are 1–2 water molecules bound to the NH_3 when it travels through the exit passage.

As shown in Figure 6A, the driving force for the first step is largely from the solvation energy of the ammonia in the water cluster in the middle of the tunnel. The barrier for this step is fairly low, so that the ammonia is able to oscillate back and forth, especially in the 9.5 ns trajectory (see Figure 3C). Similarly, in the second step, the larger solvation energy and entropy in the bulk water drive the ammonia to leave the protein and diffuse into the solvent by overcoming a 5.5 kcal/mol free-energy barrier. Technically, it is difficult to precisely estimate the free-energy profile deep into the solvent using the umbrella sampling technique. The restrains used for each window do not work as efficient as they do inside the tunnel. The end of the free-energy profile shown in Figure 6A is referring to where the ammonia is only partly solvated and close to the surface of the small subunit. However, once it passes the hydrophilic exit, the ammonia easily diffuse into the bulk water and benefits from the larger solvation energy and entropy.

A relatively low barrier of 5.7 kcal/mol (7.0–1.3 kcal/mol) for the migration from Cyg-269 to the water pocket suggests that NH_4^+ moves readily to the water pocket. However, three consecutive barriers, with free energies of 17.6, 20.3, and 22.4 kcal/mol (relative to the most stable point in the free-energy profile) along the hydrophilic passage, prevent NH_4^+ from escaping through the exit passageway (see Figure 6B). The barrier at *R* of 6.9 Å (more precisely, the plateau between the distance *R* of 5.3 and 6.9 Å) is the direct result of the repulsion between NH_4^+ and the positively charged side chain of Lys-202. For NH_4^+ to enter the water pocket, this molecule has to push away the side chain of Lys-202. Similar to NH_3, NH_4^+ is highly stabilized by the water cluster. However, the minimum appears at a distance *R* of 8.5 Å in the water pocket for NH_4^+, while it is 10.5 Å in the case of NH_3. The structures in the sampling trajectories indicate that NH_4^+ interacts strongly with these waters, so that a NH_4^+-bound water repulses Ser-35 and raises the energy of the system when it is close to Ser-35 (i.e., $R = 10.5$ Å). On the other hand, NH_3 is able to switch hydrogen bonds between water and Ser-35 more easily because of the much weaker hydrogen bonds to water relative to those between NH_4^+ and waters. Interestingly, the three consecutive barriers at distances of 13.4, 14.4, and 17.5 Å are also related to the waters surrounding NH_4^+. The NH_4^+ does not travel through the hydrophilic passage alone. Instead, it moves through this passageway with an entourage of 4–6 water molecules. The size and shape of the large $NH_4^+-H_2O$ cluster must adjust when it passes the exit port, and thus, each of the three barriers conforms to the breakage of specific hydrogen bonds. Therefore, the translocation of NH_3 from the active site in the small subunit of CPS to the large subunit is a spontaneous process and overcomes a free-energy barrier of only 5.5 kcal/mol. On the other hand, NH_4^+ is trapped in the water pocket because the passage through the tunnel in the small subunit consumes at least 17.6 kcal/mol.

Conformation and Protonation States of His-353. The initial structure, E1, yielded two successful trajectories for ammonia through the protein tunnel in 14 and 9.5 ns. The two other starting structures, D1 and D2, also resulted in the successful delivery of ammonia from the site of formation from glutamine to the water pocket in the tunnel. The ammonia moves into the water pocket at 6.25 and 0.35 ns in the cases of D1 and D2, respectively, which indicates that the movement of ammonia into the tunnel is not the rate-determining step for either of these two starting points. The

rotation of the His-353 side chain was observed together with ammonia in the two successful trajectories from structure E1 (14 and 9.5 ns), but the side chain of His-353 is basically rigid in the trajectory of D2 because a hydrogen bond forms with the carboxylate side chain of Glu-355 in the delivery process. Actually, this hydrogen bond keeps the conformation of the imidazolyl ring in His-353 unchanged in the entire trajectory. The entrance of the tunnel leading to the large subunit is open to the newly generated ammonia. The ammonia is relatively easy to break the hydrogen bond to N_ϵ of His-353 and to form a hydrogen bond to Lys-202. The ammonia keeps changing hydrogen bonds with water molecules, and the amino acid residues around it because it becomes a part of the water cluster in the middle of the tunnel. However, the rotation of the side chain of His-353 was also observed in the trajectory of D1. Accordingly, the configuration of His-353 is likely flexible as long as the ammonia is constrained in the region surrounded by Ser-47, His-353, and Lys-202. Apparently, the movement through the hydrophilic passage is the rate-determining step because the changes of the His-353 side-chain conformation and the protonated situation do not influence the exit of the ammonia. Successful trajectories were obtained for ammonia delivery from the initial structures, E1, D1, and D2, to the water pocket. Although E1 is also consistent with the X-ray crystal structure and was used to calculate the PMF, D2 more likely represents the structure consistent with the glutamine hydrolysis mechanism. The choice of the structures influences the initial delivery but not the passage of ammonia through the hydrophilic exit, which is the rate-determining step.

Mutation of Residues within the Ammonia Tunnel. Most of the residues identified in the MD simulations as being important for function in the translocation of ammonia have been mutated, and the effects on the kinetic constants for CPS have been determined. The most important of these residues appears to be Cys-269, His-353, and Ser-47. The mutation of Cys-269 to either serine or alanine results in a protein that is unable to hydrolyze glutamine (*39*). However, the C269S mutant is able to bind glutamine and stimulate the hydrolysis of ATP in the large subunit (*39*). The mutation of His-353 also results in a protein that is unable to hydrolyze glutamine (*40*). However, an X-ray structure of the H353N mutant in the presence of glutamine showed that the thioester intermediate could form but not be hydrolyzed (*41*). Thus, this residue seems to be more important for the hydrolysis of the thioester intermediate than for the formation. The hydroxyl group of Ser-47 functions as part of the oxyanion hole during the formation and hydrolysis of the thioester intermediate. Mutation of this residue to alanine results in a protein that is unable to hydrolyze glutamine in the absence of ATP/HCO_3^{2-} (*9*). However, in the presence of ATP/HCO_3^{2-}, the Michaelis constant for the glutamine is elevated by a factor of >10 but k_{cat} is largely unaffected (*9*).

Perturbations to the kinetic constants have also been observed for mutations to Lys-202 and Glu-355 (*9*). When Lys-202 is mutated to methionine, the k_{cat} values are unchanged but the K_m value for glutamine is elevated by a factor of $\sim$10. When Glu-355 is mutated to alanine, there is no change in k_{cat} but a significant increase in the K_m for glutamine (*9*). However, when this residue is mutated to glutamine, there is no detectable hydrolysis of glutamine and no carbamoyl phosphate formation (*9*).

In preliminary experiments, we have also mutated Ser-35 and Thr-37 to alanine. Ser-35 is conserved in approximately one-half of the bacterial CPS molecules, and in the other half of the sequences, this residue position is substituted with an alanine. Thr-37 is predominantly conserved, but there are a small number of substitutions with cysteine. The kinetic constants for the S35A and T37A mutants are essentially the same as the wild-type enzyme. Therefore, the role that these hydroxyl groups play in the transport of ammonia through the tunnel may be filled by additional water molecules that would occupy the space created by the mutation to alanine residues.

In comparison to the enzymatic reaction rate of several turnovers per second, the highest free-energy barrier of 5.5 kcal/mol, in our calculation, indicates that the transportation of ammonia in the small subunit apparently is not the rate-determining step. Two possibilities are raised in the S35A and T37A mutants: first, the mutations might decrease the transportation rate, but it was not able to be observed in the experiment because only the rate-determining step limits the reaction rate; second, the waters around these mutated residues might play a similar role as they do.

Conclusion. The MD simulations reported here serve as a direct demonstration of the functional existence of the molecular tunnel, which connects the small and large subunits in CPS for the transfer of NH_3 between multiple active sites. The transfer of ammonia through this tunnel is a spontaneous and fast process with a low free-energy barrier of 5.5 kcal/mol. The results on the free-energy profiles for both NH_3 and NH_4^+ transport are similar to the report by Lin et al. for NH_3/NH_4^+ transport in the AmtB membrane protein (*13*), which concludes that NH_3 travels through the tunnel with a maximum barrier of 6 kcal/mol, while NH_4^+ is completely blocked with a barrier of at least 25 kcal/mol, although PMF for NH_4^+ was not calculated for the entire reaction coordinate. His-353, Ser-47, and Lys-202 function cooperatively with one another to deliver ammonia from the site of formation in the small subunit to the interface with the large subunit via the formation and cleavage of hydrogen bonds with a critical cluster of water molecules that resides within the molecular tunnel. The NH_3 forms and breaks hydrogen bonds to Gly-292, Ser-35, Pro-358, Gly-293, and Thr-37 "macroscopically" in a stepwise fashion as it makes its way toward the exit port of the tunnel at the interface with the large subunit. The functional requirements for His-353 and Ser-35 include the formation and breakage of hydrogen bonds but also mandate that the side chains of these two residues must participate in conformational changes to enable the delivery of ammonia to the next stage of the transfer process. The driving force for the translocation of ammonia is the solvation energy of ammonia. In the site of formation, ammonia only interacts with 2–3 waters, while it is surrounded by a 5–7 water cluster in the tunnel based on the crystal structures. The expulsion of ammonia from the tunnel is induced by the complete solvation of this molecule in bulk water in the MD simulation, while a large water cluster (more than 15 waters) at the interface between the small and large subunits very likely functions in this manner in wide-type CPS. Furthermore, the chemical reaction between ammonia and the carboxyphosphate intermediate to produce carbamate provides the ultimate driving force for leading the ammonia through the entire length of the tunnel. Alternatively, NH_4^+

is unable to pass the narrow hydrophilic exit with 4–6 strongly bound waters, although this ion can be delivered to the water cluster from the active site in the small subunit of CPS. The protein in the MD simulations of the transfer of both NH_3 and NH_4^+ is significantly stable, with rmsd values of 1.18 and 1.42 Å on average, respectively. In the transport processes, only NH_3, NH_4^+, and water move freely, while all amino acid residues in the protein virtually do not change their relative positions.

Our MD simulations resulted in five successful trajectories for NH_3 transfer in the small subunit of CPS, and the subsequent PMF calculations further confirm the existence of a molecular tunnel for the translocation of NH_3 from one active site to another in the heterodimeric enzyme. This is the first time that a successful trajectory of NH_3 transport through a real tunnel (13 Å) has been obtained without artificial perturbations or elevated temperatures. Although molecular tunnels in different enzymes have been studied computationally, various artificial factors were introduced to guide the movement of NH_3 in these enzymes. For example, steered MD was used for the transfer of NH_3 in IGPS (*11, 12*), and umbrella sampling free-energy calculations were performed for NH_3 transfer in the transporter AmtB (*13*). Conventional MD simulations were carried out for AmtB but at a higher temperature of 323 K (*15*). In these simulations, the ammonia was very likely stuck to either the entrance or the terminal, which are open to the bulk water, as long as there is an energy barrier inside. The larger solvation energy and entropy in the bulk water could prevent the ammonia from moving deep inside or even draw it back to the open solvent. We anticipate that these approaches are applicable to other enzymes that use molecular tunnels to facilitate the movement of intermediates between multiple active sites.

SUPPORTING INFORMATION AVAILABLE

Computational details, analysis results, and two movies for the two successful trajectories (E1 configuration) (see Figure 2) data. This material is available free of charge via the Internet at http://pubs.acs.org.

REFERENCES

1. Raushel, F. M., Thoden, J. B., and Holden, H. M. (1999) The amidotransferase family of enzymes: Molecular machines for the production and delivery of ammonia. *Biochemistry 38*, 7891–7899.
2. Matthews, S. L., and Anderson, P. M. (1972) Evidence for the presence of two nonidentical subunits in carbamyl phosphate synthetase of *Escherichia coli*. *Biochemistry 11*, 1176–1183.
3. Trotta, P. P., Burt, M. E., Hascheme, R. H., and Meister, A. (1971) Reversible dissociation of carbamyl phosphate synthetase into a regulated synthesis subunit and a subunit required for glutamine utilization. *Proc. Natl. Acad. Sci. U.S.A. 68*, 2599–2603.
4. Thoden, J. B., Holden, H. M., Wesenberg, G., Raushel, F. M., and Rayment, I. (1997) Structure of carbamoyl phosphate synthetase: A journey of 96 Å from substrate to product. *Biochemistry 36*, 6305–6316.
5. Weeks, A., Lund, L., and Raushel, F. M. (2006) Tunneling of intermediates in enzyme-catalyzed reactions. *Curr. Opin. Chem. Biol. 10*, 465–472.
6. Mullins, L. S., and Raushel, F. M. (1999) Channeling of ammonia through the intermolecular tunnel contained within carbamoyl phosphate synthetase. *J. Am. Chem. Soc. 121*, 3803–3804.
7. Kim, J., and Raushel, F. M. (2004) Perforation of the tunnel wall in carbamoyl phosphate synthetase derails the passage of ammonia between sequential active sites. *Biochemistry 43*, 5334–5340.
8. Thoden, J. B., Huang, X. Y., Raushel, F. M., and Holden, H. M. (2002) Carbamoyl-phosphate synthetase—Creation of an escape route for ammonia. *J. Biol. Chem. 277*, 39722–39727.
9. Huang, X. Y., and Raushel, F. M. (1999) Deconstruction of the catalytic array within the amidotransferase subunit of carbamoyl phosphate synthetase. *Biochemistry 38*, 15909–15914.
10. Thoden, J. B., Huang, X. Y., Raushel, F. M., and Holden, H. M. (1999) The small subunit of carbamoyl phosphate synthetase: Snapshots along the reaction pathway. *Biochemistry 38*, 16158–16166.
11. Amaro, R., and Luthey-Schulten, Z. (2004) Molecular dynamics simulations of substrate channeling through an α-β barrel protein. *Chem. Phys. 307*, 147–155.
12. Amaro, R. E., Myers, R. S., Davisson, V. J., and Luthey-Schulten, Z. A. (2005) Structural elements in IGP synthase exclude water to optimize ammonia transfer. *Biophys. J. 89*, 475–487.
13. Lin, Y. C., Cao, Z. X., and Mo, Y. R. (2006) Molecular dynamics simulations on the *Escherichia coli* ammonia channel protein AmtB: Mechanism of ammonia/ammonium transport. *J. Am. Chem. Soc. 128*, 10876–10884.
14. Bostick, D. L., and Brooks, C. L. (2007) Deprotonation by dehydration: The origin of ammonium sensing in the AmtB channel. *PLoS Comput. Biol. 3*, 231–246.
15. Yang, H. Y., Xu, Y. C., Zhu, W. L., Chen, K. X., and Jiang, H. L. (2007) Detailed mechanism for AmtB conducting NH_4^+/NH_3: Molecular dynamics simulations. *Biophys. J. 92*, 877–885.
16. Singh, U. C., and Kollman, P. A. (1984) An approach to computing electrostatic charges for molecules. *J. Comput. Chem. 5*, 129–145.
17. Besler, B. H., Merz, K. M., and Kollman, P. A. (1990) Atomic charges derived from semiempirical methods. *J. Comput. Chem. 11*, 431–439.
18. Becke, A. D. (1988) Density-functional exchange-energy approximation with correct asymptotic behavior. *Phys. Rev. A: At., Mol., Opt. Phys. 38*, 3098–3100.
19. Lee, C. T., Yang, W. T., and Parr, R. G. (1988) Development of the Colle-Salvetti correlation-energy formula into a functional of the electron density. *Phys. Rev. B: Condens. Matter Mater. Phys. 37*, 785–789.
20. Becke, A. D. (1993) A new mixing of Hartree-Fock and local density-functional theories. *J. Chem. Phys. 98*, 1372–1377.
21. Kendall, R. A., Dunning, T. H., and Harrison, R. J. (1992) Electron affinities of the first-row atoms revisited. Systematic basis sets and wave functions. *J. Chem. Phys. 96*, 6796–6806.
22. Cances, E., Mennucci, B., and Tomasi, J. (1997) A new integral equation formalism for the polarizable continuum model: Theoretical background and applications to isotropic and anisotropic dielectrics. *J. Chem. Phys. 107*, 3032–3041.
23. Cossi, M., Barone, V., Mennucci, B., and Tomasi, J. (1998) Ab initio study of ionic solutions by a polarizable continuum dielectric model. *Chem. Phys. Lett. 286*, 253–260.
24. Mennucci, B., and Tomasi, J. (1997) Continuum solvation models: A new approach to the problem of solute's charge distribution and cavity boundaries. *J. Chem. Phys. 106*, 5151–5158.
25. Jorgensen, W. L., Chandrasekhar, J., Madura, J. D., Impey, R. W., and Klein, M. L. (1983) Comparison of simple potential functions for simulating liquid water. *J. Chem. Phys. 79*, 926–935.
26. Case, D. A., Darden, T. A., Cheatham, T. E., III, Simmerling, C. L., Wang, J., Duke, R. E., Luo, R., Merz, K. M., Pearlman, D. A., Crowley, M., Walker, R. C., Zhang, W., Wang, B., Hayik, S., Roitberg, A., Seabra, G., Wong, K. F., Paesani, F., Wu, X., Brozell, S., Tsui, V., Gohlke, H., Yang, L., Tan, C., Mongan, J., Hornak, V., Cui, G., Beroza, P., Mathews, D. H., Schafmeister, C., Ross, W. S., and Kollman, P. A. (2006) AMBER 9, University of California, San Francisco, CA.
27. Case, D. A., Darden, T. E., Cheatham, T. E., III, Simmerling, C. L., Wang, J., Duke, R. E., Luo, R., Merz, K. M., Wang, B., Pearlman, D. A., Crowley, M., Brozell, S., Tsui, V., Gohlke, H., Mongan, J., Hornak, V., Cui, G., Beroza, P., Schafmeister, C., Caldwell, J. W., Ross, W. S., and Kollman, P. A. (2004) AMBER 8, University of California, San Francisco, CA.
28. Wang, J. M., Cieplak, P., and Kollman, P. A. (2000) How well does a restrained electrostatic potential (RESP) model perform in calculating conformational energies of organic and biological molecules? *J. Comput. Chem. 21*, 1049–1074.
29. Simmerling, C., Strockbine, B., and Roitberg, A. E. (2002) All-atom structure prediction and folding simulations of a stable protein. *J. Am. Chem. Soc. 124*, 11258–11259.

30. Wang, J. M., Wolf, R. M., Caldwell, J. W., Kollman, P. A., and Case, D. A. (2004) Development and testing of a general amber force field. *J. Comput. Chem. 25*, 1157–1174.
31. Vangunsteren, W. F., and Berendsen, H. J. C. (1977) Algorithms for macromolecular dynamics and constraint dynamics. *Mol. Phys. 34*, 1311–1327.
32. Darden, T., York, D., and Pedersen, L. (1993) Particle mesh Ewald: An $N\cdot\log(N)$ method for Ewald sums in large systems. *J. Chem. Phys. 98*, 10089–10092.
33. Essmann, U., Perera, L., Berkowitz, M. L., Darden, T., Lee, H., and Pedersen, L. G. (1995) A smooth particle mesh Ewald method. *J. Chem. Phys. 103*, 8577–8593.
34. Kottalam, J., and Case, D. A. (1988) Dynamics of ligand escape from the heme pocket of myoglobin. *J. Am. Chem. Soc. 110*, 7690–7697.
35. Kumar, S., Bouzida, D., Swendsen, R. H., Kollman, P. A., and Rosenberg, J. M. (1992) The weighted histogram analysis method for free-energy calculations on biomolecules. 1. The method. *J. Comput. Chem. 13*, 1011–1021.
36. Kumar, S., Rosenberg, J. M., Bouzida, D., Swendsen, R. H., and Kollman, P. A. (1995) Multidimensional free-energy calculations using the weighted histogram analysis method. *J. Comput. Chem. 16*, 1339–1350.
37. Roux, B. (1995) The calculation of the potential of mean force using computer simulations. *Comput. Phys. Commun. 91*, 275–282.
38. Valleau, J. P., and Torrie, G. M. (1977) *Statistical Mechanics. Part A, Equilibrium Techniques*, Vol. 5, Plenum Press, New York.
39. Rubino, S. D., Nyunoya, H., and Lusty, C. J. (1986) Catalytic domains of carbamyl phosphate synthetase. Glutamine- hydrolyzing site of Escherichia coli carbamyl phosphate synthetase. *J. Biol. Chem. 262*, 11320–11327.
40. Miran, S. G., Chang, S. H., and Raushel, F. M. (1991) The role of the four conserved histidine residues in the amidotransferase domain of carbamoyl phosphate synthetase. *Biochemistry 30*, 7901–7907.
41. Thoden, J. B., Miran, S. G., Phillips, J. C., Howard, A. J., Raushel, F. M., and Holden, H. M. (1998) Carbamoyl phosphate synthetase: Caught in the act of glutamine hydrolysis. *Biochemistry 37*, 8825–8831.

BI701572H